

Blended E85–Diesel Fuel Droplet Heating and Evaporation

Nawar Al-Esawi,[†] Mansour Al Qubeissi,^{*,†,‡,§} Reece Whitaker,[‡] and Sergei S. Sazhin[§]

[†]Institute for Future Transport and Cities, Coventry University, Coventry CV1 5FB, United Kingdom

[‡]School of Mechanical, Aerospace and Automotive Engineering, Faculty of Engineering, Environment and Computing, Coventry University, Coventry CV1 2JH, United Kingdom

[§]Advanced Engineering Centre, School of Computing, Engineering, and Mathematics, University of Brighton, Brighton BN2 4GJ, United Kingdom

ABSTRACT: The multidimensional quasi-discrete (MDQD) model is applied to the analysis of heating and evaporation of mixtures of E85 (85 vol % ethanol and 15 vol % gasoline) with diesel fuel, commonly known as “E85–diesel” blends, using the universal quasi-chemical functional group activity coefficients model for the calculation of vapor pressure. The contribution of 119 components of E85–diesel fuel blends is taken into account, but replaced with smaller number of components/quasi-components, under conditions representative of diesel engines. Our results show that high fractions of E85–diesel fuel blends have a significant impact on the evolutions of droplet radii and surface temperatures. For instance, droplet lifetime and surface temperature for a blend of 50 vol % E85 and 50 vol % diesel are 23.2% and up to 3.4% less than those of pure diesel fuel, respectively. The application of the MDQD model has improved the computational efficiency significantly with minimal sacrifice to accuracy. This approach leads to a saving of up to 86.4% of CPU time when reducing the 119 components to 16 components/quasi-components without a sacrifice to the main features of the model.

1. INTRODUCTION

Diesel engines are the main power source of passenger cars and heavy duty vehicles because of their relatively high efficiency.¹ Due to the common greenhouse emissions (mainly carbon oxides and nitrogen oxides) associated with diesel engines and the depletion of fossil fuels, many investigations have been carried out on possible replacement of diesel fuel with alternatives, such as ethanol.^{2–6} Ethanol and ethanol–gasoline mixtures have been shown to be suitable for blending with diesel fuels.^{1,7} It is known that mixtures with up to 85% diesel and 15%^a ethanol are used in standard diesel engines without significant impacts on these engines.⁸ Also, it has been reported in ref 9 that ethanol can be blended with diesel fuel at up to 20% ethanol. For higher fractions of ethanol, additives may become essential to attain the needed miscibility to stabilize the blend, control the phase separation, and attain the required cetane number.^{4,8,10–13}

The most common blends of diesel fuel are not pure ethanol but 85% ethanol and 15% gasoline (E85) fuels.^{1,7,12,14} The addition of 15% gasoline to ethanol is commonly used to improve the low-temperature properties of the mixture and the cold start in diesel engines.^{12,15} The results of experimental research¹ have shown that the presence of E85 in diesel fuel leads to a noticeable reduction in nitrogen oxides. This mixture, however, has also led to a noticeable increase in the ignition delay and an increase in the production of carbon monoxides. The combustion temperature decreases with increasing the E85–diesel fuel fraction, and the brake efficiency slightly increases for higher E85–diesel fuel fractions.¹² These effects, however, need to be treated cautiously; for instance, the addition of 20% E85 can lead to up to 16% increase in nitrogen oxides.¹²

So far, research on E85–diesel fuel blends has focused on the physical properties, exhaust toxic emissions and ignition of this fuel.^{1,7,12,14} The impact of such blends, accounting for full fuel

compositions, and their detailed species chemical structure and properties, on droplet heating and evaporation has not been studied to the best of our knowledge. The importance of modeling multicomponent fuel droplet heating and evaporation processes in automotive applications has been highlighted in many studies.^{16–19} Most of the previous studies (e.g., see refs 20–22) used either the distillation curve model, assuming infinite thermal conductivity and infinite diffusivity of liquid, or the single component model, considering the initial fraction of components and ignoring the diffusivity altogether (see ref 20 for details). However, rapid evaporation of light components at the surface of the droplet leads to a high gradient of component mass fractions inside the droplet. Moreover, the temperature gradient near the droplet surface at the initial stage of droplet heating is expected to be very high due to the high ambient temperature. A number of models have been developed within the last decade to study these processes, including the discrete component (DC) model.^{16,23,24} The version of the DC model described in the latter references and used in our paper is based on the analytical solutions to the heat transfer and species diffusion equations. The DC model is generally applicable to cases when the number of components is relatively small. The application of this model, however, is expected to be computationally expensive when the number of components exceeds several dozen. To address this issue, the multidimensional quasi-discrete (MDQD) model has been suggested.²⁵

In the MDQD model, a large number of components is replaced with a much smaller number of components/quasi-components (C/QC). This approach allows one to reduce the computational time by up to 96% without substantial loss of

Received: August 30, 2018

Revised: January 26, 2019

Published: February 1, 2019

accuracy,^{26–28} which is important for the implementation of the model into commercial CFD codes (e.g., see refs 29–31). As with the DC model, the MDQD model is based on the effective thermal conductivity/effective diffusivity (ETC/ED) models to solve the heat transfer and species diffusion equations. The latter models allow one to take into account the recirculation inside the droplets, due to their relative movement, and its effect on the droplet average surface temperature and species mass fractions within a one-dimensional model.^{32,33} The DC and MDQD models have been applied to gasoline, diesel, biodiesel, and their blends.^{25–27,33–38} This paper is focused on the analysis of blended E85–diesel fuel droplets. In contrast to most previous studies, where Raoult's law was assumed to be valid (i.e., the activity coefficient (AC) was assumed to be unity), the authors of ref 39 took into account the contributions of nonunity AC, using the universal quasi-chemical functional group activity (UNIFAC) model. In this paper, the analysis of ref 39 is generalized to the case of blended E85–diesel droplets, using the DC and MDQD models. The basic equations and the compositions of fuel, used in our analysis, are described in Section 2. The validation of the model and the results predicted, using the DC and MDQD models, are presented and discussed in Section 3. The main results are summarized in Section 4.

2. MODEL AND FUEL COMPOSITIONS

Our analysis is based on the DC and MDQD models assuming that all processes are spherically symmetric. The droplet movement relevant to ambient gas (air) is considered, using the ETC/ED model.⁴⁰ The basic equations used in our analysis and fuel compositions are summarized in the following sections.

2.1. Droplet Heating. The heating of spherical droplets is described by the unsteady heat conduction equation^{41,42}

$$\frac{\partial T}{\partial t} = \kappa \left(\frac{\partial^2 T}{\partial R^2} + \frac{2}{R} \frac{\partial T}{\partial R} \right) \quad (1)$$

where $T = T(t, R)$ is the temperature in the liquid phase, t is time, R is the distance from the center of droplet, and κ is the effective thermal diffusivity^{43–45}

$$\kappa = k_{\text{eff}}/c_l \rho_l \quad (2)$$

ρ_l is the liquid density, c_l is the liquid specific heat capacity, and k_{eff} is the effective thermal conductivity (ETC), defined as^{43,45,46}

$$k_{\text{eff}} = \chi k_l \quad (3)$$

$$\chi = 1.86 + 0.86 \tanh[2.245 \log_{10}(Pe_{d(1)}/30)] \quad (4)$$

$Pe_1 = Re_{d(1)} Pr_1$, $Re_{d(1)} = \frac{2\rho_l U_s R_d}{\mu_l}$ is the droplet Reynolds number

in the liquid phase, $U_s = \frac{1}{32} \Delta U \left(\frac{\mu_g}{\mu_l} \right) Re_d C_F$ is the maximum surface velocity inside a droplet,

$$\Delta U = |U_g - U_d|, C_F = \frac{12.69}{Re_d^{2/3} (1 + B_M)}$$

is the friction drag coefficient, $Pr_1 = \frac{c_l \mu_l}{k_l}$ is the Prandtl number, U_g is the velocity of gas, U_d is the velocity of the droplet, μ_l is the liquid dynamic viscosity, k_l is the liquid thermal conductivity, Re_d is the conventional Reynolds number, and B_M is the Spalding mass transfer number defined later.¹⁶ The initial and boundary conditions for eq 1 are

$$\left. \begin{aligned} T(t=0) &= T_{d0}(R) \\ h(T_g - T_s) &= k_{\text{eff}} \frac{\partial T}{\partial R} \Big|_{R=R_d-0} \end{aligned} \right\} \quad (5)$$

where $T_s = T_s(t)$ is the droplet surface temperature, $T_g = T_g(t)$ is the ambient gas temperature, R_d is the droplet radius, and $h = h(t)$ is the convective heat transfer coefficient, found as a function of the Nusselt number Nu , as

$$h = Nu k_g / 2R_d \quad (6)$$

k_g is the thermal conductivity in the gas phase. To account for the evaporation effect on heating, the gas temperature T_g is replaced with the effective temperature T_{eff} defined as⁴⁷

$$T_{\text{eff}} = T_g + \frac{\rho_l L \dot{R}_{dE}}{h} \quad (7)$$

\dot{R}_{dE} is the droplet radius change rate due to evaporation and L is the latent heat of evaporation.

Within any given time step Δt , R_d is assumed constant and is updated at the end of Δt , as $R_{d(\text{new})} = R_{d(\text{old})} + \dot{R}_d \Delta t$, where the value of \dot{R}_d is influenced by the droplet evaporation rate and thermal swelling (see eqs 29–31).

The analytical solution to eq 1 at the end of each time step ($t = t_1$) was obtained as⁴⁸

$$\begin{aligned} T(R, t) &= \frac{R_d}{R} \sum_{n=1}^{\infty} \left\{ q_n \exp[-\kappa_R \lambda_n^2 t] - \frac{\sin \lambda_n}{\|v_n\|^2 \lambda_n^2} \mu_0(0) \right. \\ &\quad \left. \exp[-\kappa_R \lambda_n^2 t] - \frac{\sin \lambda_n}{\|v_n\|^2 \lambda_n^2} \int_0^t \frac{d\mu_0(\tau)}{d\tau} \exp[-\kappa_R \lambda_n^2 (t - \tau)] d\tau \right\} \sin \left(\lambda_n \frac{R}{R_d} \right) \\ &\quad + T_{\text{eff}}(t) \end{aligned} \quad (8)$$

where

$$\|v_n\|^2 = \frac{1}{2} \left(1 - \frac{\sin 2\lambda_n}{2\lambda_n} \right) = \frac{1}{2} \left(1 + \frac{h_{0T}}{h_{0T}^2 + \lambda_n^2} \right)$$

$$q_n = \frac{1}{R_d \|v_n\|^2} \int_0^{R_d} \tilde{T}_0(R) \sin \left(\lambda_n \frac{R}{R_d} \right) dR$$

$\tilde{T}_0(R) = R T_{d0}(R) / R_d$, $k_R = \frac{k_{\text{eff}}}{c_l \rho_l R_d^2}$, $\mu_0(t) = \frac{h T_g(t) R_d}{k_{\text{eff}}}$, and

$$h_{10} = \left(\frac{h R_d}{k_{\text{eff}}} \right) - 1.$$

A set of positive eigenvalues λ_n , $n > 0$ (the trivial solution $\lambda = 0$ is not considered), is determined from the solution to the following relation

$$\lambda \cos \lambda + h_{10} \sin \lambda = 0 \quad (9)$$

In the limit $k_{\text{eff}} \rightarrow \infty$, the prediction of expression 8 will reduce to that of the so-called “infinite thermal conductivity” model.⁴⁹ The value of Nu for an isolated moving droplet is calculated as⁴³

$$Nu_{\text{iso}} = 2 \frac{\ln(1 + B_T)}{B_T} \left[1 + \frac{(1 + Re_d Pr_1)^{1/3} \max\{1, Re_d^{0.077}\} - 1}{2F(B_T)} \right] \quad (10)$$

where $F(B_T) = (1 + B_T)^{0.7} \frac{\ln(1+B_T)}{B_T}$, B_T is the Spalding heat transfer number

$$B_T = \frac{c_{pv}(T_g - T_s)}{L_{eff}} \quad (11)$$

c_{pv} is the specific heat capacity of the fuel vapor at constant pressure

$$L_{eff} = L + \frac{Q_L}{\dot{m}_d} = \sum_i \epsilon_i L_i + \frac{Q_L}{\sum_i \dot{m}_i} \quad (12)$$

Q_L is the power spent on the droplet heating, $\epsilon_i = \epsilon_i(t)$ are the evaporation rates of species i , and $\dot{m}_i = \epsilon_i \dot{m}_d$ ($\dot{m}_d = \sum_i \dot{m}_i$). The interactions among droplets are ignored (these are discussed in refs 44, 50, and 51). The analysis of the evaporation process is based on the assumption that a mixture of vapor species and air can be treated as a separate gas (see eq 22).

2.2. Species Diffusion in the Liquid Phase. The mass fractions of liquid species $Y_{li} \equiv Y_{li}(t, R)$ are described by the transient diffusion equations for spherical droplets as⁵²

$$\frac{\partial Y_{li}}{\partial t} = D_{eff} \left(\frac{\partial^2 Y_{li}}{\partial R^2} + \frac{2}{R} \frac{\partial Y_{li}}{\partial R} \right) \quad (13)$$

where $i = 1, 2, 3, \dots$ refers to species, D_{eff} is the effective diffusivity of species in liquid phase, determined as a function of the liquid diffusivity D_1 as

$$D_{eff} = \chi_Y D_1 \quad (14)$$

coefficient χ_Y is approximated as

$$\chi_Y = 1.86 + 0.86 \tanh[2.245 \log_{10}(Re_{d(1)} Sc_{l1}/30)] \quad (15)$$

$Pe_1 = Re_{d(1)} Sc_{l1}$, $Sc_{d(1)} = \frac{\nu_1}{D_1}$ is the liquid Schmidt number, $Re_{d(1)}$ is the Reynolds number, as in eq 4, and ν_1 is the kinematic viscosity of liquid phase. The model based on eqs 13–15 is known as the effective diffusivity (ED) model.^{43,45}

The following boundary condition is considered for the solution to eq 13⁴⁰

$$\alpha(\epsilon_i - Y_{lis}) = -D_{eff} \frac{\partial Y_{li}}{\partial R} \Big|_{R=R_d-0} \quad (16)$$

where $Y_{lis} = Y_{lis}(t)$ are liquid components' mass fractions at the droplet surface

$$\alpha = \frac{|\dot{m}_d|}{4\pi\rho_1 R_d^2} = |\dot{R}_{dE}| \quad (17)$$

\dot{m}_d is the droplet evaporation rate, the calculation of which is discussed in Section 2.3 (see eq 22).

The initial condition is $Y_{li}(t=0) = Y_{li0}(R)$,

Assuming no impacts of species in the ambient gas, the values of ϵ_i were obtained as^{52–54}

$$\epsilon_i = \frac{Y_{vis}}{\sum_i Y_{vis}} \quad (18)$$

The following analytical solution to eq 13 at the end of each time step was obtained⁵²

$$Y_{li} = \epsilon_i + \frac{1}{R} \left\{ \exp\left[D_{eff} \left(\frac{\lambda_0}{R_d}\right)^2 t\right] [q_{i0} - \epsilon_i Q_0] \sinh\left(\lambda_0 \frac{R}{R_d}\right) + \sum_{n=1}^{\infty} \left[\exp\left[-D_{eff} \left(\frac{\lambda_n}{R_d}\right)^2 t\right] [q_{in} - \epsilon_i Q_n] \sin\left(\lambda_n \frac{R}{R_d}\right) \right] \right\} \quad (19)$$

where λ_0 and λ_n are calculated from $\tanh \lambda_0 = -\lambda_0/h_{0Y}$ and $\tanh \lambda_n = -\lambda_n/h_{0Y}$ (for $n \geq 1$), respectively, $h_{0Y} = -\left(1 + \frac{\alpha R_d}{D_{eff}}\right)$

$$Q_n = \left\{ \begin{array}{l} -\frac{1}{\|v_0\|^2} \left(\frac{R_d}{\lambda_0}\right)^2 (1 + h_0) \sinh \lambda_0 \text{ when } n = 0 \\ \frac{1}{\|v_n\|^2} \left(\frac{R_d}{\lambda_n}\right)^2 (1 + h_{0Y}) \sin \lambda_n \text{ when } n \geq 1 \end{array} \right\} \quad (20)$$

$\|v_n\|^2$ is obtained from eq 8, replacing h_{0T} with h_{0Y} , and

$$q_{in} = \left\{ \begin{array}{l} \frac{1}{\|v_0\|^2} \int_0^{R_d} R Y_{i0}(R) \sinh\left(\lambda_0 \frac{R}{R_d}\right) dR \text{ when } n = 0 \\ \frac{1}{\|v_n\|^2} \int_0^{R_d} R Y_{i0}(R) \sin\left(\lambda_n \frac{R}{R_d}\right) dR \text{ when } n \geq 1 \end{array} \right\} \quad (21)$$

Solution 19 is incorporated in the discrete component (DC) model, which is used in our analysis.

2.3. Droplet Evaporation. For multicomponent fuels, droplet evaporation depends on the diffusion rate of individual species in the gas phase; the evaporation rate of each component is affected by the evaporation rate of other components.^{50,52} Following refs 40 and 55, however, the relative diffusion of individual components in the gas phase is not considered. The analysis of droplet evaporation rate (\dot{m}_d) is based on the following expression

$$\dot{m}_d = -2\pi R_d D_v \rho_{total} B_M Sh_{iso} \quad (22)$$

where D_v is the binary diffusion coefficient of vapor in gas (air), $\rho_{total} = \rho_g + \rho_v$ is the total density of the mixture of vapor and gas, ρ_g is the density of the ambient gas, B_M is the Spalding mass transfer number defined as⁵⁶

$$B_M = \frac{\rho_{vs} - \rho_{v\infty}}{1 - \rho_{vs}} = \frac{Y_{vs} - Y_{v\infty}}{1 - Y_{vs}} \quad (23)$$

Y_v is the vapor mass fraction, ρ_{vs} and $\rho_{v\infty}$ are densities of vapor near the droplet surface and at a large distance from it, Sh_{iso} is the Sherwood number for isolated droplets approximated as⁴³

$$Sh_{iso} = 2 \frac{\ln(1 + B_M)}{B_M} \left[1 + \frac{(1 + Re_d Sc_d)^{1/3} \max\{1, Re_d^{0.077}\} - 1}{2F(B_M)} \right] \quad (24)$$

Sc_d is the Schmidt number for the gas phase, $F(B_M)$ is the same as in 10 but with B_T replaced with B_M .²³ B_T and B_M are linked by the following formula⁴³

$$B_T = (1 + B_M)^\phi - 1 \quad (25)$$

$$\varphi = \left(\frac{c_{pv}}{c_{pa}} \right) \left(\frac{Sh^*}{Nu^*} \right) \frac{1}{Le} \quad (26)$$

$Le = k_g / (c_{pa} \rho_g D_v)$ is the Lewis number and Sh^* and Nu^* are the modified Sherwood and Nusselt numbers, respectively, calculated as

$$Sh^* = 2 \left[1 + \frac{(1 + Re_d Sc_d)^{1/3} \max\{1, Re_d^{0.077}\} - 1}{2F(B_M)} \right] \quad (27)$$

$$Nu^* = 2 \left[1 + \frac{(1 + Re_d Pr_d)^{1/3} \max\{1, Re_d^{0.077}\} - 1}{2F(B_T)} \right] \quad (28)$$

The ratio $\frac{Sh^*}{Nu^*}$ is equal to 1 for stationary droplets. This ratio was sometimes assumed equal to 1 for slowly moving droplets.^{40,52} Such an assumption turned out to be too crude in some cases. Hence, Expressions 27 and 28 are used to estimate φ based on eq 26. Note that $\dot{m}_d \leq 0$.

When calculating the value of \dot{R}_d , both droplets evaporation and thermal swelling during the time step were taken into account⁵⁷

$$\dot{R}_d = \dot{R}_{dT} + \dot{R}_{dE} \quad (29)$$

where \dot{R}_{dT} is the rate of change in droplet radius, caused by thermal expansions or contractions, calculated as⁵⁷

$$\dot{R}_{dT} = \frac{R_d(T_{av,0})}{\Delta t} \left[\left(\frac{\rho_1(T_{av,0})}{\rho_1(T_{av,1})} \right)^{1/3} - 1 \right] \quad (30)$$

$T_{av,0}$ and $T_{av,1}$ are average droplet temperatures at the beginning $t = t_0$ and the end $t = t_1$ of the time step. The value of \dot{R}_{dE} is controlled by the droplet evaporation⁴⁰

$$\dot{R}_{dE} = \frac{\dot{m}_d}{4\pi R_d^2 \rho_1} \quad (31)$$

2.4. Species at the Droplet Surface. To find ϵ_i , the mass fractions of species in the vapor phase near the droplet surface (Y_{vis}) need to be found. The latter depend on the molar fractions of species i in the vapor phase near the droplet surface (X_{vis})⁵⁸

$$X_{vis} = X_i \frac{\gamma_i p_{vis}^*}{\varphi_i p} \quad (32)$$

where X_i is the molar fraction of the i th species in the liquid phase near the droplet surface and p_{vis}^* is the saturated vapor pressure of the i th species (in the case when $X_i = 1$, $p_{vis}^* = p_v(R_d)$), p is the ambient pressure, γ_i is the activity coefficient (AC), and φ_i is the fugacity coefficient. It has been shown, in some studies (e.g., ref 59), that the nonideality mainly originates from the liquid phase, whereas it is very low at the gas phase for the parameters used in this study. Hence, the fugacity coefficient can be assumed equal to unity, which justifies the applicability of the ideal gas law used in our analysis. In the limit when $\gamma_i = 1$ and $\varphi_i = 1$, eq 32 describes Raoult's law.⁶⁰

In contrast to previous studies, we have calculated γ_i without approximations, using the multicomponent universal quasi-chemical functional group activity coefficients (UNIFAC) model.³⁹ We have used the latter model for the prediction of

the activity coefficients of 119 components of E85–diesel fuel blends^{61,62}

$$\ln \gamma_i = \ln \gamma_i^C + \ln \gamma_i^R \quad (33)$$

where $\ln \gamma_i^C = \ln \frac{\Phi_i}{X_i} + \frac{z}{2} q_i \ln \frac{\theta_i}{\Phi_i} + l_i - \frac{\Phi_i}{X_i} \sum_j X_j l_j$,

$$\ln \gamma_i^R = \sum_k v_k^i (\ln \Gamma_k - \ln \Gamma_k^i),$$

$$l_i = \frac{z}{2} (r_i - q_i) - (r_i - 1), Z = 10, \theta_i = \frac{q_i X_i}{\sum_j q_j X_j}, Z = 10, \text{ and}$$

$$\theta_i = \frac{q_i X_i}{\sum_j q_j X_j} \text{ is the area fraction of each molecule in the mixture,}$$

$$\Phi_i = \frac{r_i X_i}{\sum_j r_j X_j} \text{ is the segment (volume) fraction of each molecule, } r_i$$

$$= \sum_k v_k^i R_k \text{ is the volume parameter, } q_i = \sum_k v_k^i Q_k \text{ is the surface parameter,}$$

$$\ln \Gamma_k = Q_k \left[1 - \ln \left(\sum_m \theta_m \psi_{mk} \right) - \sum_m \frac{\theta_m \psi_{km}}{\sum_n \theta_n \psi_{nm}} \right]$$

$$\theta_m = \frac{Q_m X_m}{\sum_n Q_n X_n} \text{ is the area fraction of group } m, X_m \text{ is the molar}$$

fraction of group m , and Q_k and R_k are the van der Waals surface areas and volumes for each functional group within a molecule, respectively,⁶ Γ_k is the residual AC of group k in the mixture and Γ_k^i is the residual AC of group k in a reference solution containing only molecules of type i , $\psi_{mn} = e^{-(a_{mn}/T)}$ is the interaction and temperature-dependent coefficient, a_{mn} is the group-interaction parameter between groups n and m , T is the interface temperature. The implementation of the UNIFAC model for the vapor pressure predictions has been validated for a highly nonideal mixture (ethanol/gasoline).³⁹

2.5. Solution Algorithm. The following algorithmic steps are used in our analysis:

1. The temperature distribution and species mass fractions are provided inside the droplet (initial homogeneous or inferred from the previous time step). The species molar fractions are converted into species mass fractions.
2. The liquid thermal conductivity and effective thermal conductivity of the droplet are calculated.
3. The partial pressures and molar fractions in the gas phase are calculated, using eq 32.
4. The Spalding mass transfer number is calculated, using eq 23.
5. The liquid heat capacity and the mixture diffusivity of vapor species in air and species evaporation rates (ϵ_i) are calculated, using eq 18.
6. The Spalding heat transfer number is calculated, using the iterations of eqs 25–28.
7. The Nusselt and Sherwood numbers are calculated for isolated droplets, using eqs 10 and 24.
8. Nu^* and Sh^* are determined, using eq 27 and 28.
9. The change of rate of droplet radius is found, using eqs 29–31.
10. The effective temperature is found, using eq 7.
11. The temperature distribution inside the droplet is found, based on eq 8, with 44 terms in the series.
12. The species distribution inside the droplet is found, based on eq 19, with 33 terms in the series.
13. The droplet radii are calculated at the end of each time step Δt . The ratio of the calculated radius to the initial radius should be higher than a priori small number of $\epsilon_s =$

10^{-6} to go to the next step; otherwise, the droplet is assumed to be completely evaporated.

14. The temperature and species distributions for the droplet with the new radius are found and used in step 1.

2.6. Fuel Compositions. The EU standard diesel fuel and gasoline for advanced combustion engines (FACE C) are used in our analysis. Diesel fuel consists of 98 hydrocarbon components, including the following mole fractions of the components: 40.0556% alkanes, 14.8795% cycloalkanes, 7.6154% bicycloalkanes, 16.1719% alkylbenzenes, 9.1537% indanes and tetralines, 8.6773% naphthalenes, 1.5647% tricycloalkanes (represented by a characteristic component $C_{19}H_{34}$), 1.2240% diaromatics (represented by a characteristic component $C_{13}H_{12}$), and 0.6577% phenanthrenes (represented by a characteristic component $C_{14}H_{10}$).²⁵ The composition of FACE C gasoline fuel (simplified from 83 to 20 hydrocarbons based on the similarity in chemical structure and thermodynamic and transport properties of components)²⁶ includes the following mole fractions of the components: 28.61% *n*-alkanes, 65.19% iso-alkanes, 4.25% alkylbenzene, 0.10% indanes (represented by C_9H_{10}), 1.49% cycloalkanes (represented by C_8H_{16}), and 0.35% olefins (represented by C_9H_{18}). Water free bioethanol (anhydrous) is used to represent “ethanol” in the fuel mixtures. Ethanol is assumed to be completely miscible in diesel (this assumption is open to question, especially for high mass fractions of ethanol due to the differences in chemical structures and characteristics of ethanol and diesel fuel).^{10,11}

The following volume fractions of E85 (85% ethanol and 15% gasoline)/diesel fuels are considered: pure diesel (i.e., 0% E85), E85-5, E85-20, E85-50, E85-80, and E85.^c As in refs 25, 26, and 33, we have taken into account the transient thermodynamic and transport properties of individual (119) components and their mixtures, which are influenced by their transient composition and ambient pressure and temperature. The fuel properties in liquid phase are determined at the droplet average temperature ($T_{av} = \frac{3}{R_d^3} \int_0^{R_d} R^2 T(R) dR$), whereas the fuel properties in gas phase are determined at the reference temperature ($T_r = \frac{2}{3}T_s + \frac{1}{3}T_g$). The ambient air density is calculated based on the ideal gas law. The latent heat of evaporation and saturated vapor pressure are calculated at T_s .

3. RESULTS

3.1. Model Validation. The results of the application of the DC model to investigate the evaporation of diesel fuel were validated against experimental data and verified against the results of other numerical simulations.^{63,64} In these papers, diesel fuel was approximated by the following components (based on their mass fractions): 8% toluene (C_7H_8), 11% decane ($C_{10}H_{22}$), 21% dodecane ($C_{12}H_{26}$), 27% tetradecane ($C_{14}H_{30}$), 17% hexadecane ($C_{16}H_{34}$), and 16% octadecane ($C_{18}H_{38}$). Droplets with initial diameters 0.86 mm (for ambient gas temperature $T = 523$ K) and 0.84 mm (for ambient gas temperature $T = 723$ K) and initial temperature of 300 K were suspended at the tip of a quartz fiber.⁶⁴ The droplet relative velocity in a chamber with an ambient pressure of 1 atm was 0.3 m/s. The ETC/ED model was used.⁶³ Note that the authors of the latter paper state that “the droplet temperature and composition were assumed to be uniform”, which would contradict their claim that they use the ETC/ED model. We

believe that this is a typo, and they refer to droplet surface temperature and composition.

The time evolutions of the normalized squared droplet diameters, predicted using our model, were compared with the numerical results presented in ref 63 and experimental data provided in ref 64. The results of the comparison are shown in Figure 1. As follows from this figure, the predictions of our code are reasonably close to the numerical and experimental data.

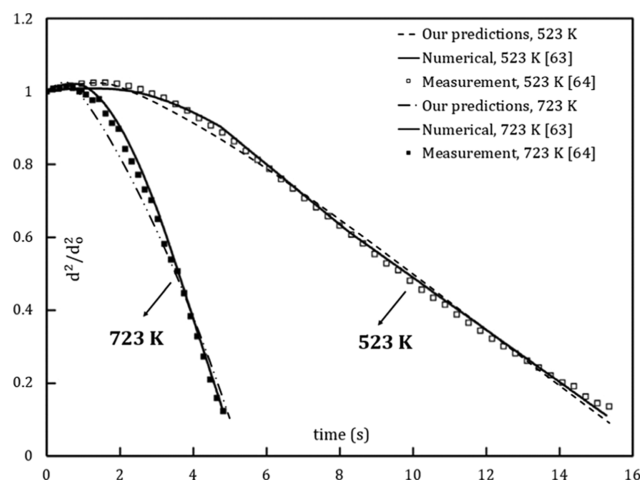


Figure 1. Normalized squared diameters of diesel fuel (represented by six-components)^{63,64} droplets versus time.

3.2. Predictions of the DC Model. The impacts of various volume fractions of E85–diesel fuel blends on droplet heating and evaporation were investigated using the DC model, where the contributions of 98, 119, and 21 components were considered for pure diesel, E85–diesel blends, and pure E85, respectively. The partial vapor pressures of the components of the blended fuel were calculated taking into account the nonunity ACs for up to 119 components using the UNIFAC model. As in refs 35 and 65, the initial droplet radius was taken equal to $R_{do} = 12.66 \mu\text{m}$, and its constant axial velocity in still air and initial temperature were assumed equal to $U_d = 10$ m/s and $T_{do} = 360$ K, respectively. The ambient air pressure and temperature were assumed constant and equal to $P = 30$ bar and $T_g = 800$ K, respectively. The time evolutions of droplet radii R_d and surface temperatures T_s for various E85–diesel fuel blends are shown in Figures 2 and 3, respectively.

As follows from Figure 2, droplet lifetime for pure diesel is longer than that for any blend. It decreases as the E85 fraction increases. The difference in droplet lifetime for E85-5 compared to pure diesel is 5.7%. This difference reaches 49.5% for pure E85. This significant reduction in droplet lifetime is ascribed to the fact that E85 is more volatile than pure diesel and has a saturation vapor pressure of 207 kPa (at $T = 360$ K), whereas it is only 2.3 kPa for pure diesel at the same temperature.

As can be seen from Figure 3, droplet surface temperature decreases with increasing E85 volume fractions. For E85-5, it is up to 0.78% less than that of pure diesel. This reduction is increased to 3.4% for E85-50 and reached 23.4% for pure E85. This difference is attributed to the fact that the heat capacity of ethanol is noticeably higher than that of diesel fuel. In agreement with the previous studies,^{27,66} droplet surface temperatures do not show plateau profiles due to the diffusion of components in droplets.

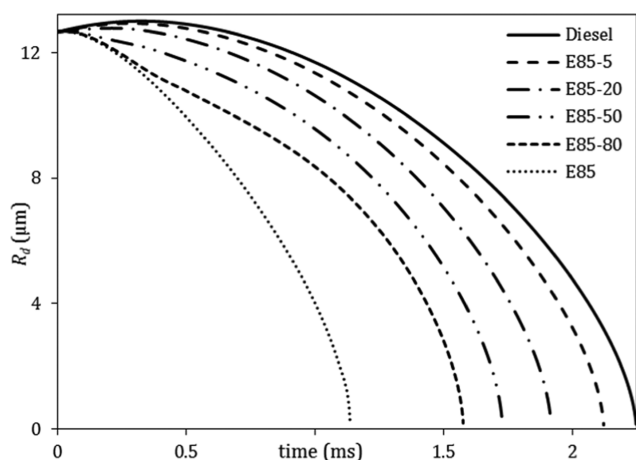


Figure 2. Droplet radii versus time for various E85–diesel blends. A droplet with an initial radius $12.66 \mu\text{m}$ and initial homogeneous temperature 360 K was assumed to be moving with a constant velocity of 10 m/s in still air. Ambient pressure and temperature were taken equal to 30 bar and 800 K , respectively.

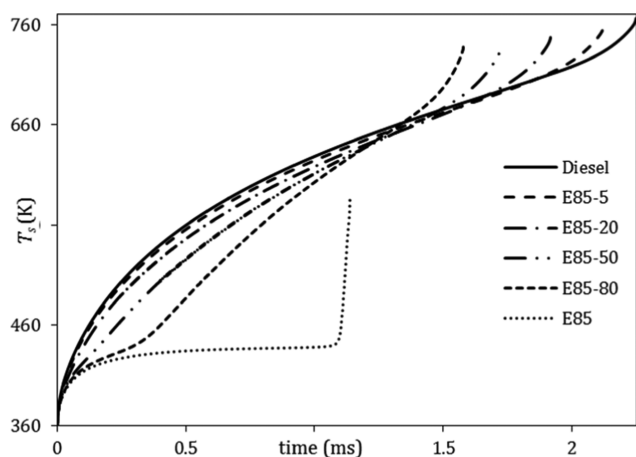


Figure 3. Droplet surface temperature versus time for various E85–diesel blends for the same ambient conditions and input parameters as in Figure 2.

The temperature distribution inside the droplet is shown in Figure 4 at time instants 0.02 , 0.3 , 0.5 , and 1 ms . As can be seen from this figure, the temperature difference between the droplet center and its surface can reach up to 9.2% . The results shown in Figure 4 should be treated with care for the case of nonzero droplet relative velocities, since the ETC/ED models were primarily developed for prediction of the average surface temperatures and species mass fractions in moving droplets.

The distillation characteristics of E85-5 and pure E85, estimated using the ETC/ED models, with the same ambient conditions as in Figures 2–4, are presented in Figure 5. As can be seen from this figure, the percentage volume recovered as distillate, for pure E85, starts at $T = 403 \text{ K}$ and ends (100% recovered) at $T = 440 \text{ K}$, which is less than the average boiling point of pure E85 at $P = 30 \text{ bar}$. For the E85-5 mixture, the percentage volume recovered starts at $T = 438 \text{ K}$ and ends at $T = 760 \text{ K}$. The sudden increase in droplet surface temperature without any volume recovered, for the latter mixture, is ascribed to the fact that the lighter components (E85) are evaporated, and the remaining are only the diesel components which start

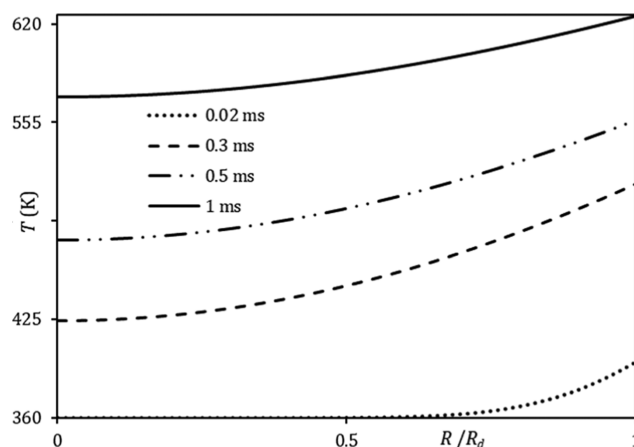


Figure 4. Temperature inside droplet versus normalized distance from the center of droplet for E85-5 blend at time instants 0.02 , 0.3 , 0.5 , and 1 ms .

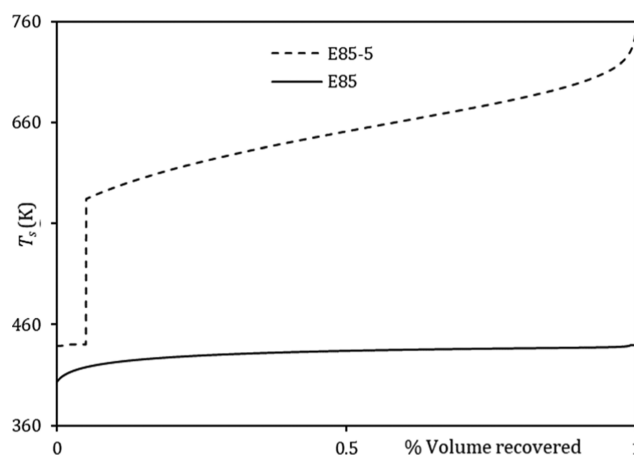


Figure 5. Droplet surface temperature versus percentage volume recovered as a distillate for E85-5 and pure E85 using the ETC/ED models.

evaporating at $T = 584 \text{ K}$. This behavior is similar to that described in ref 20.

To assess the impact of the nonideality of the liquid phase on the estimated droplet lifetimes and surface temperatures, a comparison between the results based on the two activity coefficients (the unity and UNIFAC) for E85-5 and E85-20 fuel blends is shown in Figure 6. One can see from this figure that the droplet lifetime predicted, using the UNIFAC model, is about 3.6% shorter than that based on the assumption of a unity activity coefficient. This is attributed to the fact that the nonideal mixture entails a higher vapor pressure, due to the presence of ethanol, compared to the ideal mixture. Hence, the faster evaporation rates and shorter droplet lifetimes.

The time evolution of selected 9 (out of 119) species mass fractions for E85-5 blend is shown in Figure 7. The selected components are: $\text{C}_{10}\text{H}_{22}$, $\text{C}_{19}\text{H}_{40}$, $\text{C}_{27}\text{H}_{56}$ (the alkane group), $\text{C}_{20}\text{H}_{40}$, $\text{C}_{27}\text{H}_{54}$ (the cycloalkane group), $\text{C}_{12}\text{H}_{18}$, $\text{C}_{24}\text{H}_{42}$ (the alkylbenzene group), C_8H_{18} (iso-octane in gasoline), and $\text{C}_2\text{H}_5\text{OH}$ (ethanol). As can be seen from this figure, the mass fractions of the lighter components in the blend (e.g., $\text{C}_2\text{H}_5\text{OH}$, C_8H_{18} , and $\text{C}_{10}\text{H}_{22}$) decrease monotonically with time, whereas the mass fractions of the intermediate components initially increase at the expense of lighter components and then decrease with time. The mass fractions of heavy components ($\text{C}_{27}\text{H}_{56}$ and

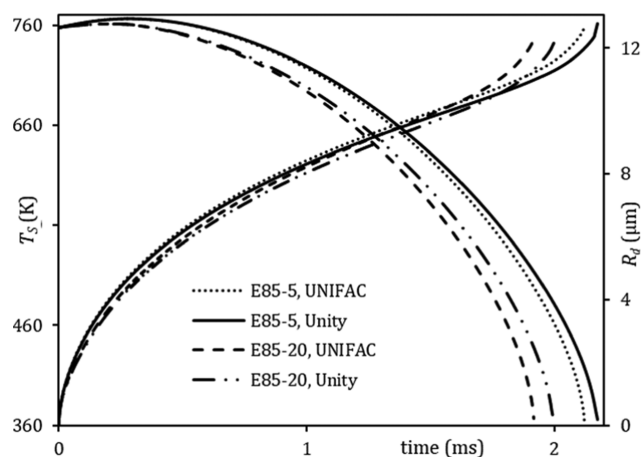


Figure 6. Evolution of droplet radii and surface temperatures for E85-5 and E85-20 blends for the same ambient conditions and input parameters as in Figures 2–5.

$C_{27}H_{54}$) increase until they become the dominant ones, although they have very small fractions initially.

3.3. Predictions of the MDQD Model. The MDQD model was used to analyze E85-5 droplets. The input parameters and ambient conditions were the same as those used for the analysis based on the DC model. The impacts of various approximations of 119 components of E85-5 blends on the predictions of droplet radii and surface temperatures are shown in Figures 8 and 9, respectively. These approximations are: 90, 63, 45, 20, and 16 components/quasi-components (C/QC) (see Appendix B for details).

As can be seen from Figures 8 and 9, the errors in droplet lifetimes and surface temperatures predicted by the model using 90 C/QC are 0.38% and up to 0.26%, respectively, compared with those predicted using the DC model taking into account the contributions of all components. These errors increase to 0.99% and up to 0.39% for droplet lifetimes and surface temperatures, respectively, when the blend is approximated by 63 C/QC. They further increase to 7.16% for droplet lifetime and up to 2.90% for the droplet surface temperature, when 16 C/QC were used. These errors are rather large for many engineering applications.

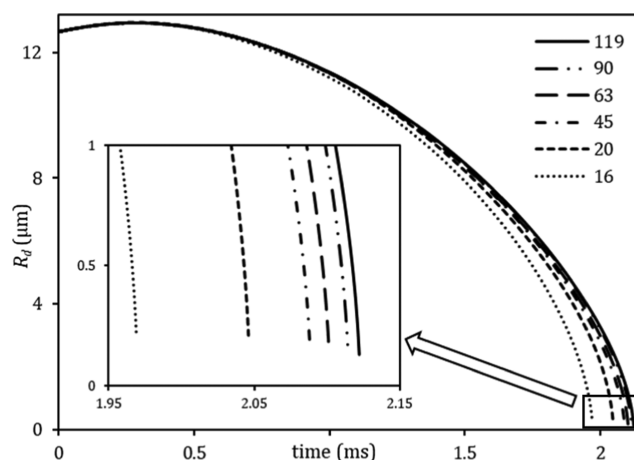


Figure 8. Droplet radii versus time for six approximations of E85-5: 119 components using the DC model and 90, 63, 45, 20, and 16 C/QC (numbers near the curves) using the MDQD model, for the same ambient conditions and input parameters as in Figures 2–7.

At the same time, it was found that the approximation of the blend by 20 C/QC underpredicts the droplet lifetimes and surface temperatures by up to 3.58% and up to 2.90%, respectively, which is acceptable in most engineering applications. The computational efficiency of the MDQD model in terms of the required CPU time is illustrated in Table 1. For example, the approximation of 119 E85-5 components by 20 components/quasi-components reduces CPU time by up to 82.7%. The workstation used is fitted with i5-3337U, dual Core, 8 GB RAM, and 1.80 GHz processor. The time step was set as 1 μ s.

4. CONCLUSIONS

The heating and evaporation of blended E85–diesel fuel droplets are investigated in conditions representative of diesel engines. It is shown that E85–diesel-blended fuel droplets have shorter lifetimes than those of pure diesel. Higher fractions of E85 result in up to 49.5% shorter droplet lifetimes and up to 23.4% lower droplet surface temperatures than those of a pure

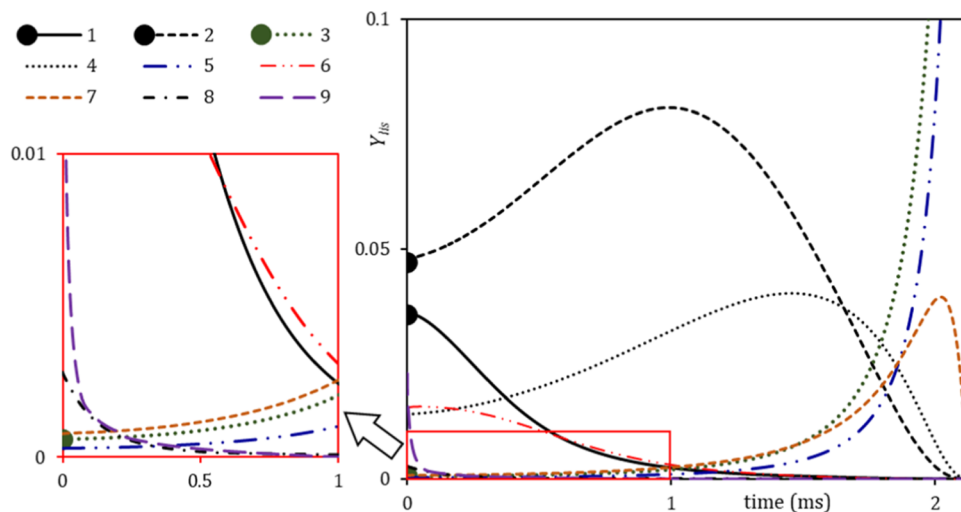


Figure 7. Plots of surface mass fractions $Y_{i/s}$ of 9 representative components of the E85-5 blend versus time. The plots for the following components are shown: $C_{10}H_{22}$ (1), $C_{19}H_{40}$ (2), $C_{27}H_{56}$ (3), $C_{20}H_{40}$ (4), $C_{27}H_{54}$ (5), $C_{12}H_{18}$ (6), $C_{24}H_{42}$ (7), C_8H_{18} (8), and C_2H_5OH (9). The same ambient conditions and input parameters as in Figures 2–6 are used.

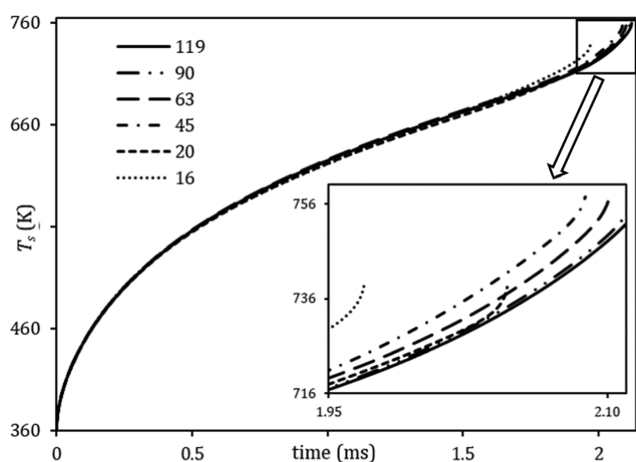


Figure 9. Droplet surface temperature versus time for six approximations of the E85-5 blend: 119 components using the DC model and 90, 63, 45, 20, and 16 C/QC (numbers near the curves) using the MDQD model, for the same ambient conditions and input parameters as in Figures 2–8.

Table 1. Impact of Using the Number of Components on

$$\text{CPU Time (diff \%)} = \frac{|\text{CPU time}_{(C/QC)} - \text{CPU time}_{119}|}{\text{CPU time}_{119}} \times 100$$

number of C/QC	CPU time (s)	diff %
119	1816	
90	1360	25.1
63	955	47.4
45	687	62.2
20	314	82.7
16	247	86.4

diesel. Such a significant impact of high E85–diesel fractions can be attributed to the differences in their saturated vapor pressure.

In the case of the E85-5 blend, the assumption of an ideal mixture with a unity activity coefficient (i.e., Raoult's law is valid) is shown to lead to an overprediction of droplet lifetimes by up to 3.6%, compared to the case when the UNIFAC activity coefficient is used.

It is shown that replacing 119 components of the blended fuel with 20 components/quasi-components reduces CPU time by up to 83% with less than 3.6 and 2.9% underpredicted droplet lifetimes and surface temperatures, respectively, compared to the prediction of the model accounting for all of the 119 components.

APPENDIX A. APPROXIMATION OF STRUCTURE GROUPS

The values of parameters R_k and Q_k for five groups in the composition of diesel fuel (bicycloalkanes, naphthalenes, tricycloalkanes, diaromatics, and phenanthrenes) are not provided anywhere, to the best of our knowledge. We have approximated the structure of these groups of molecules to the nearest available structures for which the values of parameters R_k and Q_k are known, taking into account the number of groups in each molecule. For example, when the aromatic molecule $C_{10}H_{14}$ (its structure group is available in refs 61 and 62) has 1 aromatic ring (C_6), 3 CH_2 and 1 CH_3 (the numbers 1, 3, and 1 refer to v_k^i which is the number of groups in molecule i), the diaromatic molecule $C_{12}H_{16}$ is approximated by 2 aromatic rings (C_6). Thus, the diaromatic group is approximated by 2 single

Table 2. Approximation of the Missing Structure Groups for the Predictions of the ACs^a

Group name	Group structure	
	Missing group	Approximation
Bicycloalkanes		
	The bicyclo- $C_{10}H_{18}$ is approximated by Cyclo- C_6 , 3 CH_2 and 1 CH_3 .	
Naphthalenes		
	The naphthalenes $C_{10}H_8$ is approximated by 1 aromatic C_6 , 1 CH_2 , 1 $CH=CH$ and 1 CH_3 .	
Tricycloalkanes		
	The tricycloalkane $C_{14}H_{24}$ is approximated by 2 cyclo C_6 and 2 CH_3 .	
Diaromatics		
	The diaromatic $C_{12}H_{16}$ is approximated by 2 aromatic C_6 .	
Phenanthrenes		
	The phenanthrene $C_{14}H_{11}$ is approximated by 2 aromatic C_6 and 2 CH_3 .	

^aNote that both R_k and Q_k depend on the contact distances, bond angles, bond distances, and shapes that are characteristic of the structure group.⁶⁷

aromatic groups, as shown in Table 2. This approximation allowed us to predict the activity coefficients for all components of the E85–diesel fuel blend.

APPENDIX B. APPROXIMATIONS OF THE E85–DIESEL FUEL BLEND

This appendix contains the approximations of the E85–diesel fuel blends in Table 3.

Table 3. Numbers of Components/Quasi-Components (C/QC) (Top Line) and the Compositions of C/QCs, Used in the MDQD Model for Approximating E85-5

group	119	90	63	45	20	16	
alkanes (diesel)	8	8	8	8.91 (C8–C9)	10.33 (C8–C12)	10.33 (C8–C12)	
	9	9	9				
	10	10	10	10.38 (C10–C11)			
	11	11	11				
	12	12	12	12.49 (C12–C13)			
	13	13	13		15.05 (C13–C17)	15.05 (C13–C17)	
	14	14	14	14.54 (C14–C15)			
	15	15	15				
	16	16	16	16.52 (C16–C17)			
	17	17	17				
	18	18	18	18.52 (C18–C19)	19.38 (C18–C22)	19.38 (C18–C22)	
	19	19	19				
	20	20	20	20.39 (C20–C21)			
	21	21	21				
	22	22	22	22.33 (C22–C23)			
	23	23	23		23.84 (C23–C27)	23.84 (C23–C27)	
	24	24	24	24.34 (C24–C25)			
	25	25	25				
	26	26.42 (C26–C27)	26.42 (C26–C27)	26.42 (C26–C27)	26.42 (C26–C27)		
	27						
	cycloalkanes (diesel)	10	10	10.74 (C10–C11)	10.74 (C10–C11)	12.56 (C10–C15)	12.56 (C10–C15)
		11	11				
		12	12	12.43 (C12–C13)	12.43 (C12–C13)		
		13	13				
		14	14	14.47 (C14–C15)	14.47 (C14–C15)		
		15	15				
16		16	16.49 (C16–C17)	16.49 (C16–C17)	18.29 (C16–C21)	18.29 (C16–C21)	
17		17					
18		18	18.51 (C18–C19)	18.51 (C18–C19)			
19		19					
20		20	20.35 (C20–C21)	20.35 (C20–C21)			
21		21					
22		22	22.26 (C22–C23)	22.26 (C22–C23)	22.98 (C22–C27)	22.98 (C22–C27)	
23		23					
bicycloalkanes (diesel)	10	10.60 (C10–C11)	10.60 (C10–C11)	11.1 (C10–C12)	14.74 (C10–C25)	14.74 (C10–C25)	
	11						
	12	12.40 (C12–C13)	12.40 (C12–C13)				
	13			13.86 (C13–C15)			
	14	14.43 (C14–C15)	14.43 (C14–C15)				
	15						
	16	16.57 (C16–C17)	16.57 (C16–C17)	17.09 (C16–C18)			
	17						
	18	18.60 (C18–C19)	18.60 (C18–C19)				
	19			19.31 (C19–C21)			
	20	20.32 (C20–C21)	20.32 (C20–C21)				
	21						
	22	22.41 (C22–C23)	22.41 (C22–C23)	22.92 (C22–C25)			
	23						
24	24.42 (C24–C25)	24.42 (C24–C25)					
25							
alkylbenzenes (diesel)	8	8	8.86 (C8–C9)	8.86 (C8–C9)	10.207 (C8–C13)	10.72 (C8–C16)	
	9	9					
	10	10	10.15 (C10–C11)	10.15 (C10–C11)			
	11	11					
	12	12	12.26 (C12–C13)	12.26 (C12–C13)			
	13	13					

Table 3. continued

group	119	90	63	45	20	16
	14	14	14.42 (C14–C15)	14.42 (C14–C15)	16.23 (C14–C19)	
	15	15				
	16	16	16.45 (C16–C17)	16.47 (C16–C17)		
	17	17				19.02 (C17–C24)
	18	18	18.38 (C18–C19)	18.38 (C18–C19)		
	19	19				
	20	20	20.41 (C20–C21)	20.41 (C20–C21)	21.08 (C20–C24)	
	21	21				
	22	22	22.74 (C22–C24)	22.74 (C22–C24)		
	23	23.49 (C23–C24)				
	24					
indanes and tetralines (diesel)	10	10	10.51 (C10–C11)	11.41 (C10–C13)	12.49 (C10–C16)	13.83 (C10–C22)
	11	11				
	12	12	12.47 (C12–C13)			
	13	13				
	14	14	14.45 (C14–C15)	15.34 (C14–C17)		
	15	15				
	16	16	16.46 (C16–C17)			
	17	17			18.61 (C17–C22)	
	18	18	18.39 (C18–C19)	19.24 (C18–C22)		
	19	19				
	20	20	20.57 (C20–C22)			
	21	21.32 (C21–C22)				
	22					
naphthalenes (diesel)	10	10	10.56 (C10–C11)	11.53 (C10–C15)	12.39 (C10–C20)	12.39 (C10–C20)
	11	11				
	12	12	12.35 (C12–C13)			
	13	13				
	14	14	14.44 (C14–C15)			
	15	15				
	16	16	16.42 (C16–C17)	17.90 (C16–C20)		
	17	17				
	18	18	18.98 (C18–C20)			
	19	19.51 (C19–C20)				
	20					
diesel	tricycloalkane	19	19	19		
	diaromatic	13	13	13		
	phenanthrene	14	14	14		
N-alkanes (gasoline)	4	5.24 (C4–C12)	5.24 (C4–C12)		5.24 (C4–C12)	5.24 (C4–C12)
	5					
	6			5.24 (C4–C12)		
	10					
	12					
iso-alkanes (gasoline)	4	7.37 (C4–C8)	7.37 (C4–C8)		7.37 (C4–C8)	7.41 (C4–C11)
	5					
	6			7.37 (C4–C8)		
	7					
	8					
	9	9.74 (C9–C11)	9.74 (C9–C11)	9.74 (C9–C11)	9.74 (C9–C11)	
	10					
	11					
alkylbenzenes (gasoline)	8	9.07 (C8–C11)				
	9					
	10					
	11					
gasoline	indane	9				
	cycloalkane	8				
	olefin	9				
ethanol	2	2	2	2	2	2

AUTHOR INFORMATION

Corresponding Author

*E-mail: Mansour.Qubeissi@coventry.ac.uk. Tel: +44-(0)2477-658060.

ORCID

Mansour Al Qubeissi: [0000-0001-9449-6358](https://orcid.org/0000-0001-9449-6358)

Notes

The authors declare no competing financial interest.

ACKNOWLEDGMENTS

The authors are grateful to the Institute for Future Transport and Cities, Coventry University and EPSRC (Grant EP/M002608/1) (S.S.S.) for the financial support of this project.

ADDITIONAL NOTES

^aHereafter, the percentage of substance in the mixture refers to its volume fraction, unless otherwise stated.

^bThe structure of the groups and the values of R_k and Q_k in E85–diesel fuel blends are the same as those shown in ref 39 for the ethanol–gasoline blend. Diesel fuel, however, has five more groups of molecules than gasoline fuel, namely, bicycloalkanes, naphthalenes, tricycloalkanes, diaromatics, and phenanthrenes. The approximations of these five groups are discussed in Appendix A.

^cE85–X refers to a mixture of X% volume fraction of E85 fuel and (100 – X) % volume fraction of diesel fuel.

REFERENCES

- (1) Sarjovaara, T.; Larmi, M. Dual Fuel Diesel Combustion with an E85 Ethanol/Gasoline Blend. *Fuel* **2015**, *139*, 704–714.
- (2) EPA, US. US Environmental Protection Agency. <http://www.epa.gov/> (accessed Mar 29, 2018).
- (3) U.S. Department of Energy. Ethanol Blends. https://www.eia.gov/energyexplained/index.php?page=biofuel_ethanol_use#tab2 (accessed Apr 20, 2018).
- (4) Li, D.; Zhen, H.; Xingcai, L.; Wu-gao, Z.; Jian-guang, Y. Physico-Chemical Properties of Ethanol–Diesel Blend Fuel and Its Effect on Performance and Emissions of Diesel Engines. *Renewable Energy* **2005**, *30*, 967–976.
- (5) Chin, J.-Y.; Batterman, S. A.; Northrop, W. F.; Bohac, S. V.; Assanis, D. N. Gaseous and Particulate Emissions from Diesel Engines at Idle and under Load: Comparison of Biodiesel Blend and Ultralow Sulfur Diesel Fuels. *Energy Fuels* **2012**, *26*, 6737–6748.
- (6) Liu, X.; Wang, H.; Yao, M. Experimental and Modeling Investigations on Soot Formation of Ethanol, *n*-Butanol, 2,5-Dimethylfuran, and Biodiesel in Diesel Engines. *Energy Fuels* **2017**, *31*, 12108–12119.
- (7) Tutak, W. Bioethanol E85 as a Fuel for Dual Fuel Diesel Engine. *Energy Convers. Manage.* **2014**, *86*, 39–48.
- (8) Torres-Jimenez, E.; Jerman, M. S.; Gregorc, A.; Lisec, I.; Dorado, M. P.; Kegl, B. Physical and Chemical Properties of Ethanol–Diesel Fuel Blends. *Fuel* **2011**, *90*, 795–802.
- (9) Padala, S.; Woo, C.; Kook, S.; Hawkes, E. R. Ethanol Utilisation in a Diesel Engine Using Dual-Fuelling Technology. *Fuel* **2013**, *109*, 597–607.
- (10) Satgé de Caro, P. Interest of Combining an Additive with Diesel–Ethanol Blends for Use in Diesel Engines. *Fuel* **2001**, *80*, 565–574.
- (11) Kwanchareon, P.; Luengnaruemitchai, A.; Jai-In, S. Solubility of a Diesel–Biodiesel–Ethanol Blend, Its Fuel Properties, and Its Emission Characteristics from Diesel Engine. *Fuel* **2007**, *86*, 1053–1061.
- (12) Tutak, W.; Lukács, K.; Szwaja, S.; Bereczky, Á. Alcohol–Diesel Fuel Combustion in the Compression Ignition Engine. *Fuel* **2015**, *154*, 196–206.

(13) He, B.-Q.; Shuai, S.-J.; Wang, J.-X.; He, H. The Effect of Ethanol Blended Diesel Fuels on Emissions from a Diesel Engine. *Atmos. Environ.* **2003**, *37*, 4965–4971.

(14) Curran, S.; Hanson, R.; Wagner, R. *Effect of E85 on RCCI Performance and Emissions on a Multi-Cylinder Light-Duty Diesel Engine*, SAE Technical Paper 2012-01-0376, 2012.

(15) Jeuland, N.; Montagne, X.; Gautrot, X. Potentiality of Ethanol As a Fuel for Dedicated Engine. *Oil Gas Sci. Technol.* **2004**, *59*, 559–570.

(16) Sazhin, S. S. *Droplets and Sprays*; Springer: London, 2014.

(17) Al Qubeissi, M. *Heating and Evaporation of Multi-Component Fuel Droplets*; WiSa: Stuttgart, 2015.

(18) Sazhin, S. S.; Shishkova, I. N.; Al Qubeissi, M. Heating and evaporation of a two-component droplet: hydrodynamic and kinetic models. *Int. J. Heat Mass Transfer* **2014**, *79*, 704–712.

(19) Sirignano, W. A. Fuel Droplet Vaporization and Spray Combustion Theory. *Prog. Energy Combust. Sci.* **1983**, *9*, 291–322.

(20) Hallett, W. L. H.; Beauchamp-Kiss, S. Evaporation of Single Droplets of Ethanol–Fuel Oil Mixtures. *Fuel* **2010**, *89*, 2496–2504.

(21) Laurent, C.; Lavergne, G.; Villedieu, P. Continuous Thermodynamics for Droplet Vaporization: Comparison between Gamma-PDF Model and QMoM. *C. R. Méc.* **2009**, *337*, 449–457.

(22) Burger, M.; Schmehl, R.; Prommersberger, K.; Schäfer, O.; Koch, R.; Wittig, S. Droplet Evaporation Modeling by the Distillation Curve Model: Accounting for Kerosene Fuel and Elevated Pressures. *Int. J. Heat Mass Transfer* **2003**, *46*, 4403–4412.

(23) Sazhin, S. S. Modelling of Fuel Droplet Heating and Evaporation: Recent Results and Unsolved Problems. *Fuel* **2017**, *196*, 69–101.

(24) Sazhin, S. S.; Al Qubeissi, M.; Xie, J.-F. Two Approaches to Modelling the Heating of Evaporating Droplets. *Int. Commun. Heat Mass Transfer* **2014**, *57*, 353–356.

(25) Sazhin, S. S.; Al Qubeissi, M.; Nasiri, R.; Gun'ko, V. M.; Elwardany, A. E.; Lemoine, F.; Grisch, F.; Heikal, M. R. A Multi-Dimensional Quasi-Discrete Model for the Analysis of Diesel Fuel Droplet Heating and Evaporation. *Fuel* **2014**, *129*, 238–266.

(26) Al Qubeissi, M.; Sazhin, S. S.; Turner, J.; Begg, S.; Crua, C.; Heikal, M. R. Modelling of Gasoline Fuel Droplets Heating and Evaporation. *Fuel* **2015**, *159*, 373–384.

(27) Al Qubeissi, M.; Sazhin, S. S.; Elwardany, A. E. Modelling of Blended Diesel and Biodiesel Fuel Droplet Heating and Evaporation. *Fuel* **2017**, *187*, 349–355.

(28) Al Qubeissi, M.; Sazhin, S. S.; Al-Esawi, N. In *Models for Automotive Fuel Droplets Heating and Evaporation*, The Institute for Liquid Atomization and Spray Systems (ILASS); Universitat Politècnica València: Spain, 2017; pp 1044–1051.

(29) Rybdylova, O.; Al Qubeissi, M.; Braun, M.; Crua, C.; Manin, J.; Pickett, L. M.; Sercey, G. de; Sazhina, E. M.; Sazhin, S. S.; Heikal, M. A Model for Droplet Heating and Its Implementation into ANSYS Fluent. *Int. Commun. Heat Mass Transfer* **2016**, *76*, 265–270.

(30) Rybdylova, O.; Poulton, L.; Al Qubeissi, M.; Elwardany, A. E.; Crua, C.; Khan, T.; Sazhin, S. S. A Model for Multi-Component Droplet Heating and Evaporation and Its Implementation into ANSYS Fluent. *Int. Commun. Heat Mass Transfer* **2018**, *90*, 29–33.

(31) Zaripov, T. S.; Rybdylova, O.; Sazhin, S. S. A Model for Heating and Evaporation of a Droplet Cloud and Its Implementation into ANSYS Fluent. *Int. Commun. Heat Mass Transfer* **2018**, *97*, 85–91.

(32) Al Qubeissi, M. Predictions of Droplet Heating and Evaporation: An Application to Biodiesel, Diesel, Gasoline and Blended Fuels. *Appl. Therm. Eng.* **2018**, *136*, 260–267.

(33) Al Qubeissi, M.; Al-Esawi, N.; Sazhin, S. S.; Ghaleeh, M. Ethanol/Gasoline Droplet Heating and Evaporation: Effects of Fuel Blends and Ambient Conditions. *Energy Fuels* **2018**, *32*, 6498–6506.

(34) Al Qubeissi, M.; Sazhin, S. S.; Crua, C.; Turner, J.; Heikal, M. R. Modelling of Biodiesel Fuel Droplet Heating and Evaporation: Effects of Fuel Composition. *Fuel* **2015**, *154*, 308–318.

(35) Al Qubeissi, M.; Al-Esawi, N.; Sazhin, S. S. In *Droplets Heating and Evaporation: An Application to Diesel-Biodiesel Fuel Mixtures*, The Institute for Liquid Atomization and Spray Systems (ILASS); Universitat Politècnica València: Spain, 2017; pp 1060–1067.

- (36) Al Qubeissi, M.; Al-Esawi, N.; Kolodnytska, R. Atomization of Bio-Fossil Fuel Blends. In *Advances in Biofuels and Bioenergy*; Nageswara-Rao, M., Soneji, J. R., Eds.; InTech, 2018.
- (37) Al-Esawi, N.; Al Qubeissi, M.; Sazhin, S. S. In *The Impact of Fuel Blends and Ambient Conditions on the Heating and Evaporation of Diesel and Biodiesel Fuel Droplets*, 16th International Heat Transfer Conference (IHTC16); Begellhouse: Beijing, China, 2018; pp 6641–6648.
- (38) Al Qubeissi, M.; Sazhin, S. S. In *Blended Biodiesel/Diesel Fuel Droplet Heating and Evaporation*, The Institute for Liquid Atomization and Spray Systems (ILASS), Brighton, U.K., 2016; Vol. DHE-01, p 179.
- (39) Al-Esawi, N.; Al Qubeissi, M.; Sazhin, S. S.; Whitaker, R. The Impacts of the Activity Coefficient on Heating and Evaporation of Ethanol/Gasoline Fuel Blends. *Int. Commun. Heat Mass Transfer* **2018**, *98*, 177–182.
- (40) Sazhin, S. S. Advanced Models of Fuel Droplet Heating and Evaporation. *Prog. Energy Combust. Sci.* **2006**, *32*, 162–214.
- (41) Carslaw, H. S. *Conduction of Heat in Solids*, 2nd ed.; Clarendon Press; Oxford University Press: Oxford: New York, 1986.
- (42) Sazhin, S. S.; Shishkova, I. N.; Al Qubeissi, M. A self-consistent kinetic model for droplet heating and evaporation. *Int. J. Heat Mass Transfer* **2016**, *93*, 1206–1217.
- (43) Abramzon, B.; Sirignano, W. A. Droplet vaporization model for spray combustion calculations. *Int. J. Heat Mass Transfer* **1989**, *32*, 1605–1618.
- (44) Elwardany, A. E. Modelling of Multi-Component Fuel Droplets Heating and Evaporation. Ph.D. Thesis, University of Brighton: U.K., 2012.
- (45) Abramzon, B.; Sazhin, S. S. Convective Vaporization of a Fuel Droplet with Thermal Radiation Absorption. *Fuel* **2006**, *85*, 32–46.
- (46) Sirignano, W. A. *Fluid Dynamics and Transport of Droplets and Sprays*; Cambridge University Press: Cambridge, U.K., 2010.
- (47) Sazhin, S. S.; Kristyadi, T.; Abdelghaffar, W. A.; Heikal, M. R. Models for Fuel Droplet Heating and Evaporation: Comparative Analysis. *Fuel* **2006**, *85*, 1613–1630.
- (48) Sazhin, S. S.; Krutitskii, P. A.; Abdelghaffar, W. A.; Sazhina, E. M.; Mikhailovsky, S. V.; Meikle, S. T.; Heikal, M. R. Transient Heating of Diesel Fuel Droplets. *Int. J. Heat Mass Transfer* **2004**, *47*, 3327–3340.
- (49) Sazhin, S. S.; Krutitskii, P. A. In *A Conduction Model for Transient Heating of Fuel Droplets*, Proceedings of the 3rd ISAAC Congress, World Scientific: River Edge, NJ, 2003; pp 1231–1240.
- (50) Maqua, C.; Castanet, G.; Grisch, F.; Lemoine, F.; Kristyadi, T.; Sazhin, S. S. Monodisperse Droplet Heating and Evaporation: Experimental Study and Modelling. *Int. J. Heat Mass Transfer* **2008**, *51*, 3932–3945.
- (51) Sazhin, S. S.; Elwardany, A. E.; Krutitskii, P. A.; Deprédurand, V.; Castanet, G.; Lemoine, F.; Sazhina, E. M.; Heikal, M. R. Multi-Component Droplet Heating and Evaporation: Numerical Simulation versus Experimental Data. *Int. J. Therm. Sci.* **2011**, *50*, 1164–1180.
- (52) Sazhin, S. S.; Elwardany, A.; Krutitskii, P. A.; Castanet, G.; Lemoine, F.; Sazhina, E. M.; Heikal, M. R. A Simplified Model for Bi-Component Droplet Heating and Evaporation. *Int. J. Heat Mass Transfer* **2010**, *53*, 4495–4505.
- (53) Continillo, G.; Sirignano, W. A. Unsteady, Spherically-Symmetric Flame Propagation Through Multicomponent Fuel Spray Clouds. In *Modern Research Topics in Aerospace Propulsion*; Angelino, G., Luca, L. D., Sirignano, W. A., Eds.; Springer: New York, 1991; pp 173–198.
- (54) Faeth, G. M. Evaporation and Combustion of Sprays. *Prog. Energy Combust. Sci.* **1983**, *9*, 1–76.
- (55) Deprédurand, V.; Castanet, G.; Lemoine, F. Heat and Mass Transfer in Evaporating Droplets in Interaction: Influence of the Fuel. *Int. J. Heat Mass Transfer* **2010**, *53*, 3495–3502.
- (56) Spalding, D. B. *Convective Mass Transfer: An Introduction*; Edward Arnold Publ. Ltd: London, 1963.
- (57) Sazhin, S. S.; Abdelghaffar, W. A.; Krutitskii, P. A.; Sazhina, E. M.; Heikal, M. R. New Approaches to Numerical Modelling of Droplet Transient Heating and Evaporation. *Int. J. Heat Mass Transfer* **2005**, *48*, 4215–4228.
- (58) Atkins, P. W.; De Paula, J. *Atkins' Physical Chemistry*; Oxford University Press: Oxford, 2002.
- (59) Bader, A.; Keller, P.; Hasse, C. The Influence of Non-Ideal Vapor–Liquid Equilibrium on the Evaporation of Ethanol/Iso-Octane Droplets. *Int. J. Heat Mass Transfer* **2013**, *64*, 547–558.
- (60) Rogers, M. C.; Brown, G. G. Raoult's Law and the Equilibrium Vaporization of Hydrocarbon Mixtures. *Ind. Eng. Chem.* **1930**, *22*, 258–264.
- (61) Poling, B. E.; Prausnitz, J. M.; O'Connell, J. P. *The Properties of Gases and Liquids*; McGraw-Hill: New York, 2001.
- (62) Reid, R. C.; Prausnitz, J. M.; Poling, B. E. *The Properties of Gases and Liquids*, 4th ed.; McGraw-Hill: New York, 1987.
- (63) Ni, Z.; Han, K.; Zhao, C.; Chen, H.; Pang, B. Numerical Simulation of Droplet Evaporation Characteristics of Multi-Component Acetone-Butanol-Ethanol and Diesel Blends under Different Environments. *Fuel* **2018**, *230*, 27–36.
- (64) Ma, X.; Zhang, F.; Han, K.; Yang, B.; Song, G. Evaporation Characteristics of Acetone–Butanol–Ethanol and Diesel Blends Droplets at High Ambient Temperatures. *Fuel* **2015**, *160*, 43–49.
- (65) Al Qubeissi, M.; Sazhin, S. S. Models for droplet heating and evaporation: an application to biodiesel, diesel and gasoline fuels. *Int. J. Eng. Syst. Modell. Simul.* **2017**, *9*, 32–40.
- (66) Sazhin, S. S.; Al Qubeissi, M.; Heikal, M. R. In *Modelling of Biodiesel and Diesel Fuel Droplet Heating and Evaporation*, 15th International Heat Transfer Conference; Begellhouse: Kyoto, Japan, 2014; IHTC15-8936.
- (67) Bondi, A. Van Der Waals Volumes and Radii. *J. Phys. Chem.* **1964**, *68*, 441–451.